Electrochemistry of S Adlayers at Underpotentially Deposited Cd on Au(111): Implications for the Electrosynthesis of High-Quality CdS Thin Films

Anthony Gichuhi, B. Edward Boone, Umit Demir,† and Curtis Shannon*

Department of Chemistry, Auburn University, Auburn, Alabama 36849-5312

Received: January 6, 1998; In Final Form: May 16, 1998

We report an electrochemical, scanning probe microscopic, and Raman spectroscopic investigation of thin CdS films grown by electrochemical atomic layer epitaxy aimed at understanding the role played by the order of deposition on film quality. Using scanning tunneling microscopy (STM), we determine the atomic level structure of the first three monolayers of CdS for Cd-first films. The initial Cd underpotential deposition layer forms a stable $\begin{pmatrix} 4 & -2 \\ 0 & 1 \end{pmatrix}$−Au(111) adlattice in which the two unique nearest neighbor spacings are 0.33 and 0.29 nm. When H_2S is electrolyzed at this surface at underpotential, an adlattice is produced in which the S−S interatomic spacing is 0.34 nm. The unit cell of this structure is $\begin{pmatrix} 4 & -2 \\ 0 & 2 \end{pmatrix}$ with respect to Au(111). Both the Cd and S monolayers appear to be nearly closest-packed, in contrast to the more open structures observed in the S-first films. Interestingly, the second monolayers of Cd and S were found to have the same structure as in the first monolayer of CdS, implying that the first two CdS monolayers are epitaxial. Only after deposition of the third monolayer of CdS are interatomic spacings characteristic of bulk CdS observed. Micrometer-resolution STM images reveal a significant decrease in pit density, average pit diameter, and average pit depth for the Cd-first films compared to that for the S-first films. Finally, resonance Raman data indicate that S-first films are significantly more polydisperse than Cd-first films. Taken together, these data point to a structural rearrangement in the first monolayer of CdS as the origin of the increased polycrystallinity in the S-first films. In contrast, the closest-packed structures formed when Cd is deposited first lead to films with fewer defects. The implications of these findings on the electrosynthesis of thin film materials is briefly discussed.

Introduction

The electrosynthesis of thin film materials offers several advantages over traditional synthetic approaches, including experimental simplicity and the ability to work under ambient conditions.[1] Most electrosynthetic schemes, however, suffer from two decisive disadvantages. First, the deposits tend to be highly polycrystalline[2] because nucleation and growth, adsorption/desorption phenomena, surface reconstruction, and surface diffusion typically are not under experimental control. Second, electrodeposited materials tend to be relatively impure due to the incorporation of components of the supporting electrolyte into the deposit as it forms. New approaches to electrosynthesis based on underpotential deposition (UPD) promise to overcome at least some of these difficulties. For example, UPD is a surface-limited process; consequently, film growth is governed by two-dimensional as opposed to three-dimensional growth kinetics. In addition, UPD is a cooperative phenomenon and leads to the formation of well-ordered monolayer structures. The electrochemical behavior and physical properties of UPD monolayers have been studied extensively, and several reviews have appeared in the literature.[3] More recently, scanning probe microscopy studies have revealed many of the atomic level details of UPD.[4]

Stickney and co-workers were the first to systematically study the use of UPD to grow compounds on surfaces. Their work has led to the development of an electrochemical analogue to atomic layer epitaxy (EC-ALE).[5] In the simplest implementation of EC-ALE, a thin film of the target compound is produced by sequential UPD of its elemental components. This method has been most successfully applied to the growth of relatively polar materials possessing a simple one-to-one stoichiometry, such as CdTe,[6] CdSe,[7] and ZnS.[8] Thin semiconductor films synthesized by EC-ALE have proved to be particularly interesting from a spectroscopic point of view because of the precise control of film thickness afforded by this method. Spectroscopic investigations of CdS films grown by EC-ALE have facilitated studies of charge carrier transport through electrosynthesized materials[9] and have allowed the study of quantum confinement effects in ultrathin films.[10]

In a series of earlier papers on the growth of CdS thin films on Au, we reported on the kinetics of CdS monolayer formation[11] as well as on the influence of the substrate crystallographic orientation on the structure of the deposit. When an atomic layer of sulfur is underpotentially deposited on Au(111)[12] or Au(100),[13] for example, a stable $(\sqrt{3} \times \sqrt{3})$R30° or $(\sqrt{2} \times \sqrt{2})$R45° sulfur adlattice, respectively, is formed. When cadmium is deposited at underpotential on either of these sulfur-modified surfaces, the thermodynamic product (i.e., wurtzite CdS) is produced. In particular, the cubic form of CdS is not observed on the 4-fold symmetric $(\sqrt{2} \times \sqrt{2})$R45°-S/Au(100) surface despite the excellent lattice matching between cubic CdS and Au(100).

To our knowledge, in all previously reported EC-ALE syntheses, the more electronegative nonmetal is deposited as

* Address correspondence to this author. Tel: 334-844-6964. Fax: 334-844-6959. E-mail: shanncg@mail.auburn.edu.

† Present address: Department of Chemistry, Faculty of Arts and Sciences, Ataturk University, 25240 Erzurum, Turkey.

S1089-5647(98)00657-9 CCC: $15.00
Published on Web 07/31/1998

the initial layer, followed by deposition of the more electropositive metallic element. This is done to mitigate against possible alloy formation between the working electrode, which is typically a noble metal, and the deposited metal. Here, we report an electrochemical, scanning tunneling microscopic, and Raman spectroscopic study of the atomic level structure and long-range order of CdS monolayer and multilayer films formed when Cd is the initial element deposited in the EC-ALE cycle. Several investigations of Cd UPD on metal electrodes focusing on fundamental issues as well as electrocatalysis have been reported.[14] In particular, a recent study by Gewirth and Nuzzo[15] on Cd UPD identified several stable, potential-dependent Cd UPD structures on Au(111), suggesting that a Cd-first EC-ALE cycle would be feasible. Using scanning tunneling microscopy (STM), we identify a $\begin{pmatrix} 4 & -2 \\ 0 & 1 \end{pmatrix}$−Cd/Au(111) UPD layer that is stable to emersion under potential control and transfer to an H_2S-containing electrolyte. Cyclic voltammetry of the Cd-modified electrode in H_2S demonstrates that CdS can be grown in a monolayer-by-monolayer fashion. An S overlayer is observed which is $\begin{pmatrix} 4 & -2 \\ 0 & 2 \end{pmatrix}$ with respect to Au(111). Interestingly, interatomic spacings characteristic with wurtzite CdS are not observed by STM until the third CdS layer has been deposited. Finally, resonance Raman spectroscopy and micrometer-resolution STM were used to probe the degree of order within the films and demonstrate that films in which Cd is deposited first are significantly more highly ordered than those formed when S is deposited first.

Experimental Section

Preparation of Au(111) Substrates. The Au microbead electrodes used in this study were prepared using literature methods.[16] These substrates are polycrystalline, but typically contain numerous large elliptical (111) facets with major and minor axis lengths of approximately 1000 μm and 500 μm, respectively. These substrates can be aligned for STM imaging using a low-magnification optical microscope.

Chemicals. $3CdSO_4 \cdot 8H_2O$, $Na_2S \cdot 9H_2O$, $NaClO_4 \cdot H_2O$, $HClO_4$, and H_2SO_4 (Certified ACS Plus) were used as received. Millipore-Q purified water was used to make up all solutions.

Electrochemistry. Electrochemistry experiments were carried out in a single-compartment, three-electrode Teflon cell. Ag/AgCl (3 M NaCl) was the reference electrode, to which all electrode potentials are referred; the counterelectrode was a platinum wire. Cyclic voltammetry was performed using a Pine AFRDE-4 bipotentiostat and an HP-7055B X-Y recorder. The electrochemical cell was directly connected to a solution-handling manifold that allowed the electrolyte to be changed without the working electrode being exposed to the ambient. The solution reservoirs and all components that came into contact with the solutions were made of Teflon or Kel-F. All solutions were purged for 20 min with ultrahigh purity (UHP) Ar to remove O_2.

No attempt was made to record the voltammetry associated with an individual (111) facet on the microbead electrode; thus, all cyclic voltammograms are characteristic of a polycrystalline sample. The substrate was thoroughly rinsed with blank electrolyte solution following the deposition of each element. After the final deposition cycle, the substrates were emersed under potential control, dried in a stream of UHP Ar and stored under UHP Ar prior to imaging.

Cadmium deposition was carried out from a 1 mM $CdSO_4$ solution (pH 2.9) prepared from $3CdSO_4 \cdot 8H_2O$ in 0.1 M H_2SO_4. To deposit the first monolayer of Cd, the electrode potential was scanned from +0.800 to −0.560 V at a scan rate of 0.100 V s^{-1}. The second and third monolayers of Cd were deposited at a fixed potential of −0.500 V. Sulfide was deposited from a solution prepared from 1 mM $Na_2S \cdot 9H_2O$ in 0.1 M $NaClO_4 \cdot H_2O$/0.01 M $HClO_4$ supporting electrolyte. Sulfide solutions were prepared fresh prior to each experiment due to the evolution of H_2S at this acidic pH (2.5−2.9). The first monolayer of S was deposited by sweeping the electrode potential from −0.630 to −0.300 V at 0.100 V s^{-1}. The second and third monolayers of S were formed at fixed electrode potentials of −0.200 and −0.350 V, respectively.

Scanning Tunneling Microscopy. All STM experiments were performed in air using a Model SA-1 ambient STM (Park Scientific Instruments, Sunnyvale, CA). Atomic- and micrometer-scale images were acquired using either constant height (micrometer-resolution) or constant current (atomic-resolution) modes. In all cases, W tips, prepared by etching a 0.5 mm diameter wire in 1 M KOH solution using a commercial etching circuit, were used for imaging, and the tip was biased positive relative to the sample. The calibration of the piezoelectric scanner in the $x-y$ plane was performed using two different standards: highly oriented pyrolytic graphite (HOPG, donated by Dr. Arthur Moore, Union Carbide, Parma, OH) and a Au(111) single crystal. The standard deviation for all the lateral dimensions reported here is ±0.014 nm. The z-calibration (perpendicular to the plane of the surface) of the piezo was carried out using the Au atomic step height (0.235 nm). Some of the images (Figure 2d,f) were moderately filtered using a Wiener filter routine supplied by the manufacturer to remove high-frequency noise.

Resonance Raman Spectroscopy. The resonance Raman spectrometer used for this work has been described previously.[9] Briefly, Raman scattering was excited using the 488.0 and 457.6 nm lines of a Coherent Innova-70 Ar^+ laser. Continuous wave power levels at the CdS samples were maintained at ca. 200 mW. The incident light was p-polarized (p-, in the plane of incidence) and was focused to an approximately 100 μm spot on the CdS surface using a spherical lens. The angle of incidence was approximately 40−50° with respect to the surface normal. The scattered radiation was collected using a f-matched f/1.4 camera lens (Canon). The instrumental slit width was approximately 5 cm^{-1} in all spectra, and the acquisition time per spectrum was typically 250 s.

Results and Discussion

Electrochemistry. The cyclic voltammetric traces for the deposition of the first three EC-ALE monolayers of CdS onto a polycrystalline Au microbead electrode are shown in Figure 1a−f, where the sequence of voltammograms corresponds to the order in which the elements were deposited. The voltammograms are intended to illustrate the voltammetric response of each surface and to indicate how the deposition potentials were chosen. They are not intended to imply that a complete UPD-stripping cycle was performed prior to the deposition of each element. Elemental deposition was carried out as described in the Experimental Section and in the discussion of the STM images which follows. The deposition of the initial Cd monolayer was carried out at underpotential from 0.1 M H_2SO_4 supporting electrolyte at a naked Au electrode, Figure 1a. This voltammetry is qualitatively the same as what was reported by Gewirth and Nuzzo for Cd UPD at a Au(111) single crystal carried out under the same conditions.[14] These workers identified three potential-dependent Cd UPD structures on Au(111). The large cathodic and anodic waves centered at −0.100 V correspond to the initial underpotential deposition and

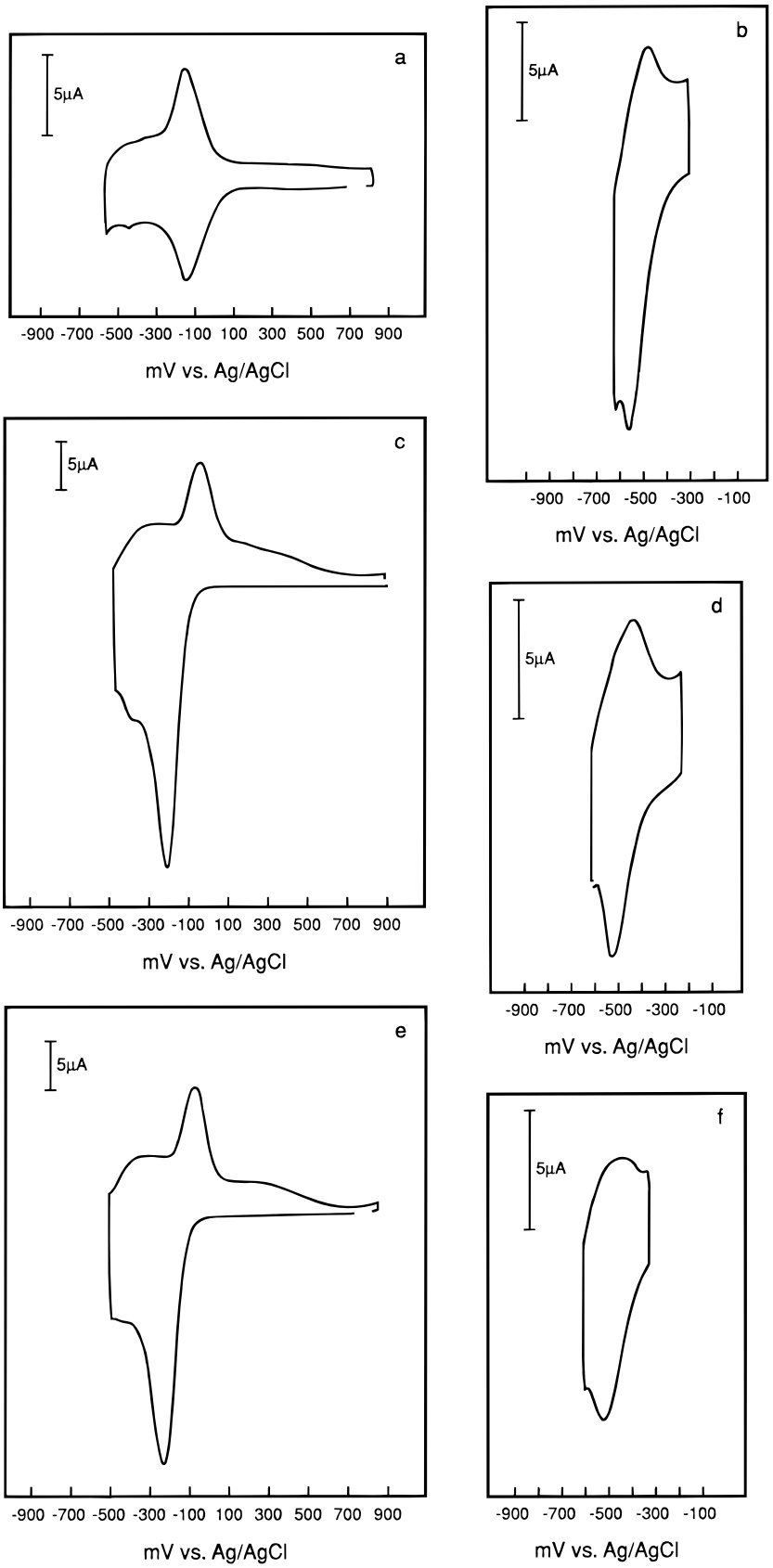

Figure 1. Cyclic voltammetric behavior of Cd and S in the underpotential deposition region at naked and modified Au surfaces. The data were used to determine the deposition conditions for the growth of the first three monolayers of CdS. (a) Underpotential deposition of Cd at naked Au. (b) Deposition of the first monolayer of S on Cd/Au. (c) Deposition of the second monolayer of Cd on one monolayer of CdS/Au. (d) Deposition of the second monolayer of S. (e) Deposition of the third monolayer of Cd on two monolayers of CdS/Au. (f) Deposition of the third monolayer of S. Note that in all cases the scan rate was 0.100 V s^{-1} and the electrode area was 0.071 cm^2.

stripping of Cd, while the small features at more negative potentials are due to the formation and dissolution of higher density phases. The deposition and stripping of the second and third monolayers of Cd are shown in Figure 1 parts c and e,

TABLE 1: Summary of Voltammetric and Structural Data

cycle	element	peak	potential (mV)	ΔE_p (mV)	$E^{0\prime}$ (mV)	q (μC cm^{-2})	θ_{coul}	θ_{STM}	structure
first	Cd	E_a	-100 ± 5			277 ± 5	0.62		
				0 ± 5	-100			0.67	$\begin{pmatrix} 4 & -2 \\ 0 & 1 \end{pmatrix}$
		E_c	-100 ± 5			272 ± 5	0.61		
	S	E_a	-480 ± 4			*a*			
				93 ± 3	-527			0.68	$\begin{pmatrix} 4 & -2 \\ 0 & 2 \end{pmatrix}$
		E_c	-573 ± 7			309 ± 12	0.69		
second	Cd	E_a	-89 ± 2			262 ± 7	0.58		
				135 ± 2	-157			0.67	$\begin{pmatrix} 4 & -2 \\ 0 & 1 \end{pmatrix}$
		E_c	-224 ± 4			*a*			
	S	E_a	-454 ± 4			*a*			
				103 ± 2	-506			0.68	$\begin{pmatrix} 4 & -2 \\ 0 & 2 \end{pmatrix}$
		E_c	-557 ± 6			269 ± 10	0.61		
third	Cd	E_a	-76 ± 2			242 ± 6	0.54		6-fold, $d_{Cd-Cd} = 0.38$ nm
				164 ± 3	-158			0.55	
		E_c	-240 ± 5			*a*			
	S	E_a	-446 ± 5			*a*			
				97 ± 1	-494			0.47	6-fold, $d_{S-S} = 0.42$ nm
		E_c	-543 ± 4			207 ± 6	0.46		

[a] These values could not accurately be determined.

respectively. We observe three general trends in comparing the voltammetry of Cd at a S-modified surface to the UPD on naked Au. First, there is a significant negative shift of $E^{0\prime}$ for deposition at either of the two S-modified surfaces as compared to deposition at naked Au, which is consistent with the formation of CdS. Second, there is a monotonic increase in ΔE_p from the first to the third monolayer deposited which is indicative of slow electron-transfer kinetics through the thicker CdS films. Recent secondary ion mass spectrometry (SIMS) data indicate, in fact, that S-terminated CdS(0001) behaves as an electrical insulator.[17] It should be noted that the Cd voltammetry at the S-terminated surfaces reported here differs somewhat from our previous reports in that the voltammetric peaks are sharper and the stripping wave occurs at a more negative potential. These differences appear to be due solely to the different electrolyte compositions used in the two studies and are completely reproducible. Third, integration of the Cd stripping wave indicates that different amounts of Cd are deposited in each subsequent EC-ALE cycle.

Sulfur was deposited from solutions prepared by dissolving sodium sulfide in 0.1 M $NaClO_4 \cdot H_2O$/0.01 M $HClO_4$ supporting electrolyte. At this pH (2.5−2.9), which was chosen to closely match the pH of the Cd electrolyte (ca. 2.9), the dominant sulfur-containing species in solution is H_2S. The voltammetric behavior of H_2S at each of the first three Cd monolayers is shown in Figure 1 parts b, d, and f. The H_2S voltammetry is qualitatively different from that observed at higher pHs in that the potentials are shifted significantly positive and that a single voltammetric wave is observed as opposed to the two waves that are typically seen in basic media. The origin of these differences is quite complex and will be discussed more fully in a forthcoming report.[18] The voltammetric data for the deposition of the first three monolayers of CdS are summarized in Table 1.

Scanning Probe Microscopy. Atomic-resolution STM images were obtained in air immediately after each deposition cycle and are presented in Figure 2. Imaging was performed on one of the large (111) facets on the surface of the gold microbead electrode. To deposit the first monolayer of Cd, the electrode potential was scanned from +0.800 to −0.560 V at a scan rate of 0.100 V s^{-1}. The working electrode was removed under potential control, rinsed with pure electrolyte, and dried in a stream of UHP Ar before transfer to the scanning tunneling microscope for imaging. The stability of the Cd UPD layer to emersion was confirmed by carrying out stripping voltammetry in pure electrolyte. The coulometric coverages calculated in these experiments were found to be equal to the values determined in the Cd electrolyte itself and indicate that no Cd is lost from the surface during the emersion step. Figure 2a shows a 5.0 nm by 5.0 nm STM image of the Cd overlayer formed under these conditions. This image shows a 2-fold symmetric arrangement of atoms in which the two unique nearest neighbor distances are 0.33 and 0.29 nm as measured along the long and short unit vectors, respectively. The interatomic distances in this monolayer are very close to the van der Waals radius of Cd of 0.298 nm[19] which suggests that this structure represents essentially saturation coverage of Cd on Au(111). The proposed structure of this overlayer is shown in Figure 3a. In this adlattice, which is $\begin{pmatrix} 4 & -2 \\ 0 & 1 \end{pmatrix}$ with respect to the Au(111) substrate, half of the atoms occupy atop sites and half occupy 3-fold hollow sites on Au(111). In addition, the angle between the adsorbate lattice vectors is 90° as compared to an angle of 60° between the substrate lattice vectors. The coverage associated with this overlayer is 0.67, in excellent agreement with our coulometric results (Table 1) and recent chronocoulometric data.[20] It should be noted that this type of overlayer structure was not observed by Gewirth and Nuzzo in their study of Cd UPD on Au(111). All of the Cd UPD structures observed by these workers were found to display long-range order along an axis rotated 30° with respect to one of the substrate lattice directions. Although the $\begin{pmatrix} 4 & -2 \\ 0 & 1 \end{pmatrix}$ structure we observe does not exhibit a banded morphology, we did observe a uniaxially symmetric overlayer structure when the electrode was emersed at −0.290 V. The differences in the structures reported here and those reported previously is likely due to the coadsorption of sulfate which recent quartz crystal microbalance experiments have shown to be strongly adsorbed.[18] Consequently, it may also be that not all of the spots in our STM image correspond to Cd atoms.

The electrodeposition of a monolayer of S on the Cd-modified Au electrode was carried out by scanning the potential from an initial value of −0.630 V to a final potential of −0.300 V using a scan rate of 0.100 V s^{-1}. The STM image shown in Figure 2b is representative of the atomic level structure we observe on this surface. This 5.0 nm by 5.0 nm image shows a lattice in which the S−S interatomic distance is 0.34 nm. As with the initial Cd layer, the atoms appear to pack at close to their van der Waals distances ($d_{vdW}^{Sulfur} = 0.35$ nm).[19] The assignment

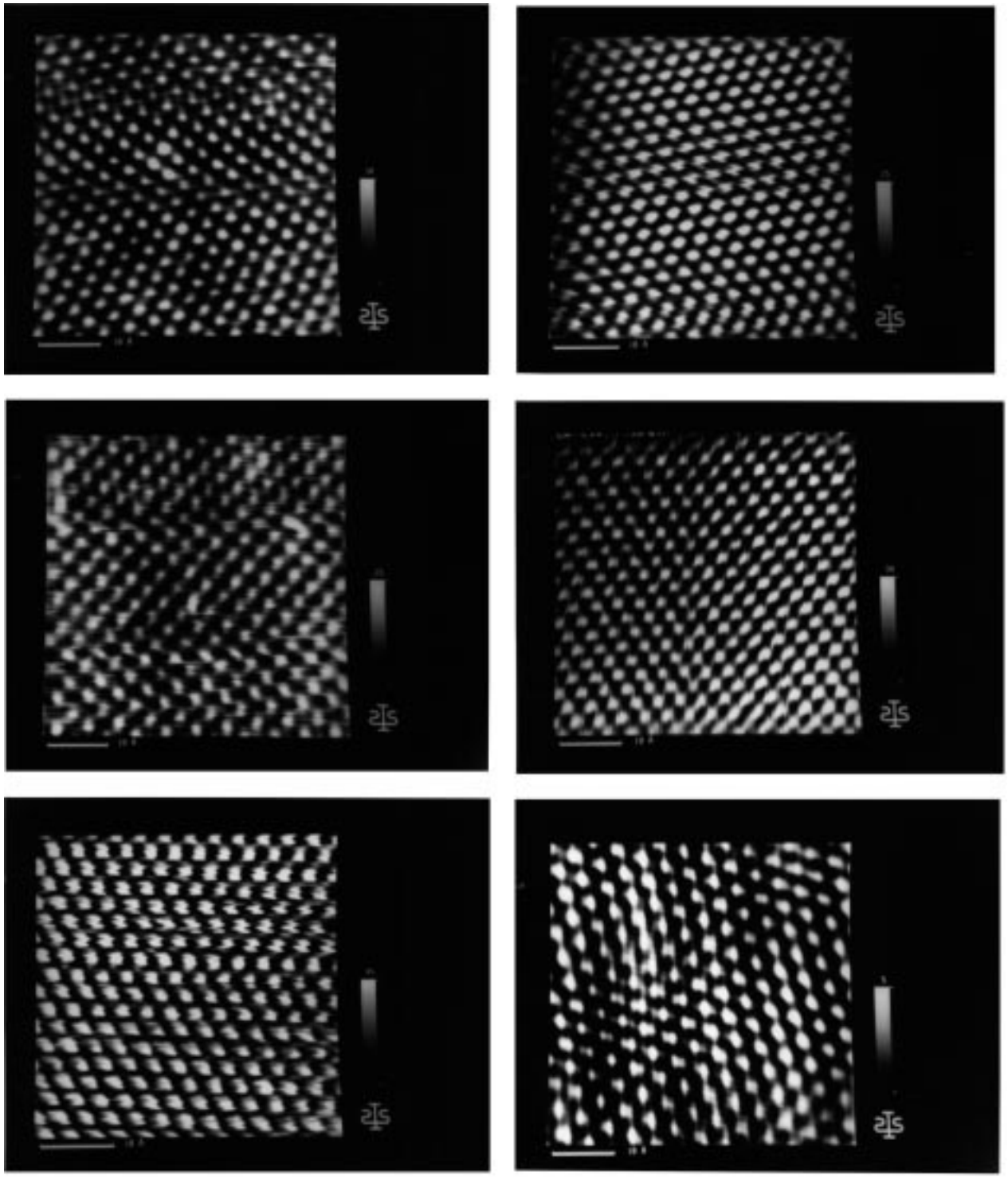

Figure 2. Atomic-resolution STM images of the first three monolayers of CdS on Au(111). The images were acquired immediately after the deposition cycles shown in Figure 1. (a) The first monolayer of Cd. (b) The first monolayer of S. (c) The second monolayer of Cd. (d) The second monolayer of S. (e) The third monolayer of Cd. (f) The third monolayer of S.

of the S adlayer structure will be discussed below. We turn first to a discussion of the second monolayer of CdS. Interestingly, at the atomic scale, the structures observed after the deposition of the second Cd and S monolayers are identical to what we observed in the first monolayer. Representative 5.0 nm by 5.0 nm STM images of these two surfaces are shown, respectively, parts c and d in Figure 2. One possible, though unlikely, explanation for this observation is that these images correspond to regions of the surface where the first Cd and S monolayers are somehow exposed. This possibility was ruled out for the following reasons: first, these films are characterized by a very low defect density (see below and Table 2); second, the coverage associated with each deposition cycle appears to be close to saturation for both elements; third, Auger electron spectroscopy (AES) shows a linear dependence of the Cd AES signal at 382 eV on the number of monolayers deposited. The fact that the first two monolayers of CdS are identical does, however, have an important implication. This observation strongly suggests that first four monolayers deposited (that is, the first two CdS monolayers) are commensurate. If this were

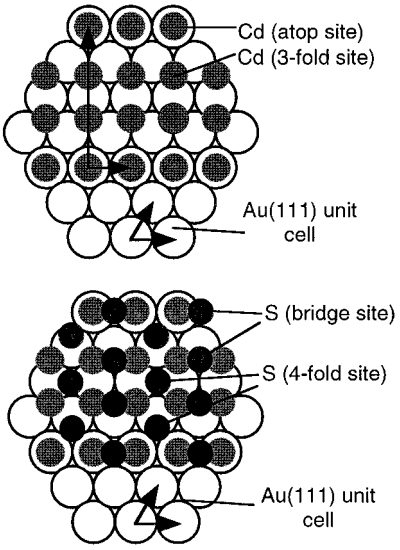

Figure 3. (a) Proposed structure of the first two Cd monolayers. (b) Proposed structure of the first two monolayers of S. See text for details.

TABLE 2: STM Analysis of CdS Monolayer Defects

	Cd-first	S-first
One Monolayer		
average pit density (μm^{-2})	109 ± 151	260 ± 173
average pit depth (nm)	0.241 ± 0.061	0.406 ± 0.17
average pit diameter (nm)	31.2 ± 23	57.2 ± 56
rms roughness (nm)	0.064 ± 0.009	0.294 ± 0.21
Two Monolayers		
average pit density (μm^{-2})	236 ± 87	1634 ± 107
average pit depth (nm)	0.427 ± 0.011	0.508 ± 0.08
average pit diameter (nm)	0.309 ± 0.10	18.9 ± 2.4
rms roughness (nm)	0.140 ± 0.041	0.157 ± 0.072
Three Monolayers		
average pit density (μm^{-2})	903 ± 52	1707 ± 450
average pit depth (nm)	1.10 ± 0.14	*a*
average pit diameter (nm)	13.4 ± 1.6	*a*
rms roughness (nm)	0.368 ± 0.032	0.445 ± 0.215

[a] Could not accurately be determined due to the highly polycrystalline nature of the sample.

not the case, that is, if the first S overlayer were incommensurate with respect to the initially deposited Cd UPD layer, then the second Cd layer would be expected to display a unique atomic level structure determined by this incommensurate layer, which is not the case. The structure of the two S overlayers is $\begin{pmatrix} 4 & -2 \\ 0 & 2 \end{pmatrix}$ with respect to the Au(111) substrate. The proposed S overlayer structure is shown schematically in Figure 3b. In this model, S atoms are shown bridging two Cd adatoms and located in 4-fold hollows in the Cd adlattice. In addition, this model predicts a single S−S bond distance of 0.33 nm which is within experimental error of the observed *d* spacing of 0.34 nm.

Interesting structural differences emerge when the third layers of Cd and S are deposited, as shown in Figure 2e,f. In contrast to the closest-packed structures characteristic of the first two monolayers, the third Cd monolayer forms a more open 6-fold symmetric lattice in which the interatomic spacing is 0.38 nm; when the third layer of S atoms is deposited, an interatomic spacing of 0.42 nm is observed. This spacing corresponds to the characteristic S−S distance in the CdS(0001) plane. The STM data are summarized and compared to the electrochemical results in Table 1.

Resonance Raman Spectroscopy and Micrometer-Resolution STM. Resonance Raman spectroscopy was used to confirm the formation of CdS and to probe the degree of polydispersity of the films produced as a function of deposition

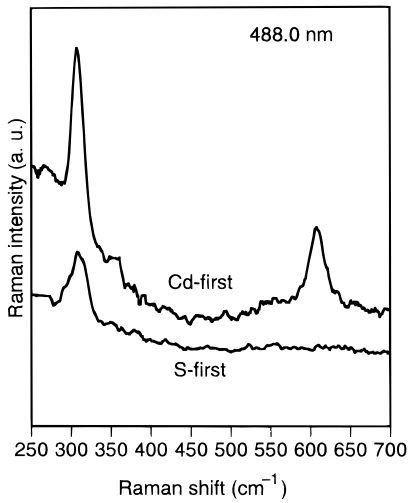

Figure 4. Resonance Raman spectra obtained using 488.0 nm excitation for four cycles of CdS deposited Cd-first (upper trace) and S-first (lower trace).

order. Representative spectra collected for S-first and Cd-first films are shown in Figure 4. Although a measurable signal can be detected from a single monolayer of CdS when Cd is deposited first, the detection limit is 2−3 CdS monolayers in the S-first films due to a change in the Raman scattering mechanism (see below). For this reason, spectra were acquired from samples consisting of four complete EC-ALE cycles of CdS. The peak centered at ca. 305 cm^{-1} is the longitudinal optical phonon mode of the CdS lattice (1LO) and the feature at approximately 600 cm^{-1} is the overtone of this mode (2LO). Observation of the phonon spectra confirm that CdS is being formed in both instances. Two additional differences between the spectra can be identified. First, the Raman line widths are significantly broader in the S-first films as compared to the Cd-first films. In the former case, the fwhm of the fundamental band averages 27 cm^{-1}, while in the latter case the average fwhm is only 18 cm^{-1}. The difference in line width corresponds to an increased inhomogeneous broadening due to a wider distribution of crystallite sizes when S is deposited first. The increased polydispersity in the S-first films is due to a structural rearrangement of the $(\sqrt{3} \times \sqrt{3})$R30°-S monolayer upon UPD of Cd. As CdS forms, the S−S nearest neighbor spacing changes from 0.50 nm in the $(\sqrt{3} \times \sqrt{3})$R30° overlayer to 0.42 nm in the CdS crystallites, a compression of about 29% in the unit cell area. In contrast, there is no possibility of such a structural rearrangement in the Cd-first films when S is deposited because the Cd UPD overlayer is essentially closest packed. Thus, a film characterized by a high degree of long-range order is produced when Cd is the first element deposited in the cycle. The second significant difference between the resonance Raman spectra in Figure 4 is that the overtone mode is not observed in the Raman spectrum of the S-first film. Previous work by our group[10] as well as by others[21] has shown that the intensity of the overtone band depends on two variables: the degree of quantum confinement of the sample and the dephasing of the electronic excited state. In the case of extremely thin films such as these, however, the relative intensity of the overtone mode is only related to the degree of quantum confinement. Therefore, changes in the overtone intensity at a constant excitation wavelength are related to the degree of detuning between the laser line used to excite Raman scattering and the CdS thin film absorption maximum. The spectra in Figure 4 show that the laser wavelength is close to being on-resonance in the case of the Cd-first films (intense overtone) and is highly detuned in

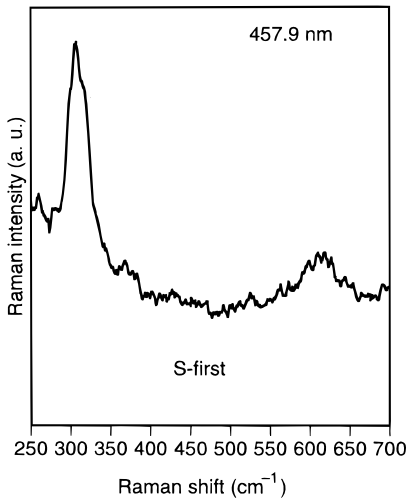

Figure 5. Resonance Raman spectra obtained using 457.9 nm excitation for four cycles of CdS deposited S-first.

the case of the S-first films (overtone absent). In other words, the spectrum of the Cd-first film represents resonance Raman scattering while the S-first spectrum is normal Raman scattering. As further evidence for this interpretation, when the S-first film is excited at 457.9 nm the overtone intensity increases, Figure 5. This result suggests that the absorption maximum of the S-first film is blue-shifted with respect to that of the Cd-first film and is consistent with an increased polydispersity in the S-first films. That is, the S-first films can be thought of as consisting of small platelets of CdS while the Cd-first films are essentially contiguous in the plane of the surface. A detailed discussion of quantum confinement effects in these films will appear elsewhere.[9]

Micrometer-scale STM imaging provides additional evidence for long-range structural differences between the two films. Representative images of a single monolayer of CdS grown Cd-first and S-first are shown in Figure 6 parts a and b, respectively. The increased long-range structural order of the Cd-first films is apparent by inspection of these images.

Quantitative structural information obtained from micrometer-scale STM images is presented in Table 2. This table also includes a summary of preliminary STM experiments on the second and third monolayers of CdS.[22] These data, which were compiled by averaging multiple ($\geq$10) line scans on at least 5 different STM images in each case, show several distinct trends. First, all of the measures of monolayer disorder increase as the number of monolayers deposited increases, regardless of which element is deposited first. Particularly striking in this regard are the changes in the average pit density. That the average pit density increases as the number of monolayers deposited increases is not surprising, and is, in fact, consistent with the propagation of defects within the film as subsequent monolayers are deposited onto a substrate that itself contains defects. For instance, we observe a monotonic increase in the average pit density in the Cd-first films. In contrast, there is a much more dramatic increase in the average pit density at the second monolayer in the case of the S-first films. Again, we believe this is explained by the structural changes that occur as the first monolayer of Cd is deposited onto the $(\sqrt{3} \times \sqrt{3})$R30°-S adlattice, as discussed earlier. As a consequence, the first EC-ALE cycle results in submonolayer coverage of CdS. Thus, the second EC-ALE cycle likely involves both growth on exposed Au (i.e., "filling in") as well as growth on the first CdS monolayer. It should be noted, however, that in all cases the root mean square (rms) roughness (and to a lesser extent, the average pit depth) remains comparable to the CdS *d* spacing of 0.34 nm. This indicates that precipitation from solution is not an important growth mode and that the differences in the film structure are related to the EC-ALE mechanism.

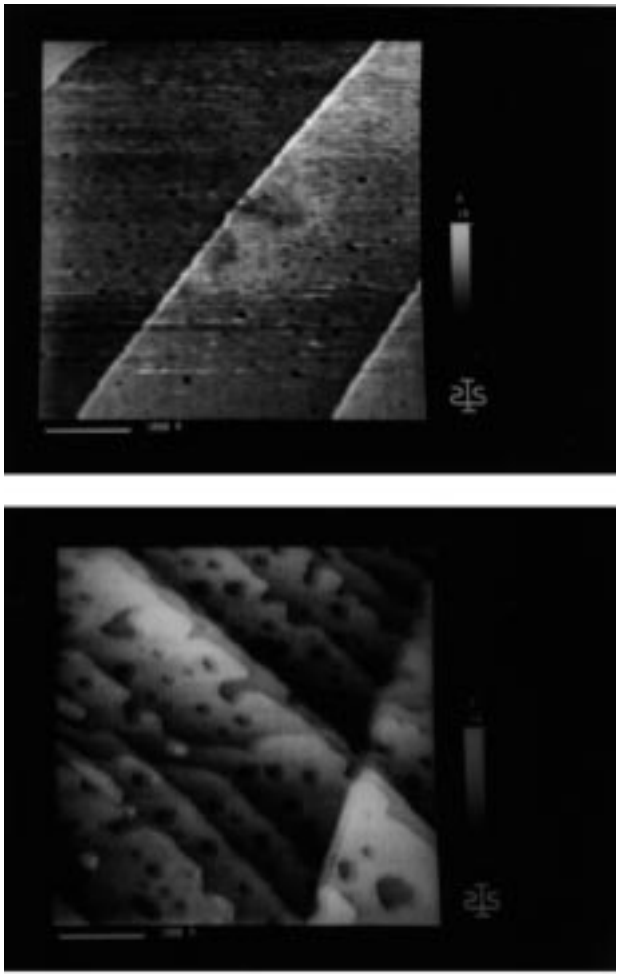

Figure 6. Micrometer-resolution STM images obtained for one monolayer of CdS deposited (a) Cd-first and (b) S-first.

Conclusions

We have studied the influence of the order of deposition on the atomic level structure and long-range order of CdS films grown by electrochemical atomic layer epitaxy. We find that the order of deposition plays a very significant role in terms of the atomic level structure of the UPD overlayers and the long-range order of the films. Specifically, the S-first films are significantly more polycrystalline than the Cd-first films. At the atomic level, this behavior can be understood as arising from a structural rearrangement in the S-first films as the first monolayer of CdS forms. On the other hand, when Cd is deposited first, the closest-packed UPD overlayer is sterically constrained from undergoing such a reconstruction. As a consequence, the long-range order of the Cd-first films is significantly higher. Currently, we are investigating the optical and spectroscopic properties of these films and will report our findings in the near future.

Acknowledgment. Auger electron spectroscopy experiments were performed by Prof. M. J. Bozack (Department of Physics, Auburn University). The financial support of this work by the National Science Foundation (OSR-9557748) and Auburn University is gratefully acknowledged.

References and Notes

(1) (a) Pandey, R. K., Sahu, S. N., Chandra, S., Eds. *Handbook of Semiconductor Electrodeposition*; Marcel Dekker: New York, 1996. (b) Lokhande, C. D.; Yermune, V. S.; Pawar, S. H. *J. Electrochem. Soc*. **1991**, *138*, 624. (c) Dona, J. M.; Herrero, J. *J. Electrochem. Soc.* **1992**, *139*, 2810. (d) Dona, J. M.; Herrero, J. *J. Electrochem. Soc*. **1994**, *141*, 205. (e) Froment, M.; Bernard, M. C.; Cortes, R. *J. Electrochem. Soc*. **1995**, *142*, 2642.

(2) (a) Chen, J. H.; Wan, C. C. *J. Electroanal. Chem*. **1994**, *365*, 87. (b) Das, S. K.; Morris, G. C. *Sol. Energy Mater. Sol. Cells* **1993**, *30*, 107. (c) Bouroushian, M.; Loïzos, Z.; Spyrellis, N., Maurin, G. *Thin Solid Films* **1993**, *229*, 101. (d) De Mattei, R. C.; Feigelson, R. S. In *Electrochemistry of Semiconductors and Electronics: Processes and Devices;* McHardy, J., Ludwig, F., Eds.; Noyes: Park Ridge, NJ, 1992; p 1. (e) Shearson, P. C. *Sol. Energy Mater. Sol. Cells* **1992**, *27*, 377. (f) Cataldi, T. R. I.; Blackham, I. G.; Briggs, G. A. D.; Pethica, J. B.; Hill, H. A. O. *J. Electroanal. Chem*. **1990**, *290*, 1. (g) Lokhande, C. D.; Pawar, S. H. *Phys. Status Solidi A* **1989**, *111*, 17. (h) Falop, G. F.; Taylor, R. M. *Annu. Rev. Mater. Sci*. **1985**, *15*, 197. (i) Loïzos, Z. R.; Spyrellis, N.; Maurin, G. *Thin Solid Films* **1991,** 204, 139. (j) Sahn, S. N.; Sanchez, C. *Solid State Commun.* **1990**, *73*, 597.

(3) (a) Leiva, E. *Electrochim. Acta* **1996**, *41*, 2185. (b) Kolb, D. M. In *Advances in Electrochemistry and Electrochemical Engineering*; Gerisher, H., Tobias, C. W., Eds.; Wiley-Interscience: New York, 1978; Vol. 11, p 125. (c) Adzic, R. In *Advances in Electrochemistry and Electrochemical Engineering*; Gerischer, H., Tobias, C. W., Eds.; Wiley-Interscience: New York, 1984; Vol. 13, p 159. (d) Juttner, K.; Lorenz, W. J. Z. *Phys. Chem*. (Wiesbaden) **1980**, *122*, 163. (e) Green, M. P.; Hanson, K. J.; Carr, R.; Lindau, I. *J. Electrochem. Soc* **1990**, *137*, 3493. (f) Green, M. P.; Hanson, K. J.; Scherson, D. A.; Xing, X.; Richter, M.; Ross, P. N.; Carr, R.; Lindau, I. *J. Phys. Chem*. **1989**, *93*, 2181.

(4) Gewirth, A. A.; Niece, B. K. *Chem. Rev.* **1997**, *97*, 1129.

(5) (a) Colletti, L. P.; Thomas, S.; Wilmer, E. M.; Stickney, J. L. *Mater. Res. Soc. Symp. Proc*. **1997**, *451*, 235. (b) Gregory, B. W.; Stickney, J. L. *J. Electroanal. Chem.* **1991**, *300*, 543. (c) Villegas, I.; Stickney, J. L.; *J. Electrochem. Soc.* **1992**, *139*, 686. (d) Suggs, D. W.; Stickney, J. L. *Surf. Sci.* **1993**, *290*, 362. (e) Colletti, L. P.; Teklay, D.; Stickney, J. L. *J. Electroanal. Chem.* **1994**, *369*, 145.

(6) Suggs, D. W.; Stickney, J. L. *Surf. Sci*. **1993**, *290*, 375.

(7) Stickney, J. L.; Villegas, I.; Gregory, B. W.; Suggs, D. W. *J. Vac. Sci. Technol*. **1992**, *A10*, 886.

(8) Gichuhi, A.; Shannon, C. *Langmuir*, submitted. See also ref 5a.

(9) Boone, B. E.; Shannon, C. *J. Phys. Chem.* **1996**, *100*, 9480.

(10) Boone, B. E.; Gichuhi, A.; Shannon, C. *J. Phys. Chem. B*, submitted.

(11) Demir, U.; Shannon, C. *Langmuir* **1996**, *12*, 6091.

(12) Demir, U.; Shannon, C. *Langmuir* **1994**, *10*, 2794.

(13) Demir, U.; Shannon, C. *Langmuir* **1996**, *12*, 594.

(14) (a) Huang, H.; Zhao, M.; Xing, X.; Bai, I. T.; Scherson, D. *J. Electroanal. Chem. Interfacial Electrochem.* **1990**, *293*, 279. (b) Machado, S. A. S.; Tanaka, A. A.; Gonzalez, E. R. *Electrochim. Acta* **1992**, *37*, 2559. (c) Martins, M. E.; Hernandez-Creus, A.; Salvarezza, R. C.; Arvia, A. J. *J. Electroanal. Chem.* **1994**, *375*, 141. (d) Tang, Y.; Furtak, T. E. *Electrochim. Acta* **1991**, *36*, 1873. (e) Xing, X.; Bae, I. T.; Scherson, D. A. *Electrochim. Acta* **1995**, *40*, 29. (f) Xing, X. K.; Scherson, D. A. *J. Electroanal. Chem. Interfacial Electrochem.* **1985**, *196*, 439.

(15) Bondos, J. C.; Gewirth, A. A.; Nuzzo, R. G. *J. Phys. Chem*. **1996**, *100*, 8617.

(16) Hsu, T. *Ultramicroscopy* **1988**, *11*, 167.

(17) Prof. Scott S. Perry, University of Houston, private communication.

(18) Gichuhi, A.; Shannon, C. *J. Electrochem. Soc*., submitted.

(19) Kittel, C. *Introduction to Solid State Physics*, 6th ed.; John Wiley and Sons: New York, 1986.

(20) Niece, B. K.; Gewirth, A. A. *Langmuir* **1997**, *13*, 6302.

(21) Shiang, J. J.; Risbud, S. H.; Alivisatos, A. P. *J. Chem. Phys*. **1993**, *98*, 8432.

(22) Gichuhi, A.; Shannon, C. *J. Electrochem. Soc*., in preparation.